Remote Health Monitoring System for Bedbound Patients

Mostafa Alizadeh (m5alizad@uwaterloo.ca)
University of Waterloo https://orcid.org/0000-0002-8260-7716
George Shaker
University of Waterloo
Safieddin Safavi-Naeini
University of Waterloo

Research Article

Keywords: COVID-19, FMCW radar, MIMO, respiration monitoring, CFAR, mean shift clustering, harmonic analysis, remote monitoring, vital signs

Posted Date: July 22nd, 2020

DOI: https://doi.org/10.21203/rs.3.rs-46286/v1

Abstract

There are many patients who require continuous monitoring of vital signs and their sleep position such as bedbound patients and hospitalized patients. Also, in some cases, like COVID-19, it is critical for a caregiver to keep a safe distance to the patient. For remote monitoring, radar technologies have been shown to be promising. Thus, in this paper, we present a novel solution for the remote breath and sleep position monitoring by using a multi-input-multi-output (MIMO) radar. Our proposed system could monitor a number of people simultaneously, and therein we use a high-resolution direction of arrival (DOA) detection for finding close targets. Furthermore, the sleep position of each target is determined using a support vector machine (SVM) classifier. The breath analysis involves designing an optimum filter for estimating both the breathing rate and the noiseless breathing waveform. Furthermore, we tested the system by hand-made targets and real human targets. The radar placed in a bedroom environment above a bed where two subjects were sleeping next to each other. For the breathing rate, the accuracy of the radar is more than 97% for human subjects compared with a reference sensor. Also, the sleep position correct detection is more than 83%.

Introduction

COVID-19 outbreak has tremendously changed the world in many ways, but it learns us many lessons to adapt and maintain sustainability in pandemics. The protection of healthcare providers must be the first priority. However, due to the exponential increment of the number of patients, plus the shortage of personal protection equipment (PPE) create a huge challenge to control the pandemic. In addition, body temperature, blood oxygen density, heartbeats, and respiration are the primary vital signs that they are monitored constantly in the hospitals for COVID-19 patients, but the conventional medical devices require attachments of a part to the patient's body. Thus, instead of reducing risk to the hospital workers, they increase the risk of infection to the healthcare providers. So, we need to employ new technologies for long-distance monitoring of multiple patients. This reduces the exposure and cost, and it overcomes the shortage in PPEs by reducing the number of nurses.

Sleep apnea, bedsore, sleep disorders, and, in general, bedbound patients require various wearable or contact medical tools to record vital signs. Sleep monitoring with the polysomnography (PSG) as a gold standard is very costly and requires the continuous supervision of a physician. Mostly, these are contact devices intervening with the patients' freedom. Although in some cases, the devices are impossible to be connected to the patient; for instance –a patient with burned skin. Indeed, health monitoring is interrupted when the attachments become loose, or at least, the measurement error increases. However, more convenience and reliability can be offered by contactless devices. For instance, it has been shown that radars can detect vital signs without any contact with the body by capturing tiny chest motions due to cardiorespiratory activity[1–4]. Although they can facilitate non-obstructive, touchless, and long-term vital signs detection, practically using radars for heart rate and breathing rate (BR) detection lacks enough accuracy in the presence of body motions[1] or the radar platform motion[4]. In particular, they can be used

for bedbound patients where they are supposed to be stationary most of the time with occasional movements.

Remote vital signs monitoring with radars covers a number of areas ranging from electric and magnetic characterizations of human body[5–9] to high resolution spectral and temporal signal acquisition and detection[10–13]. For the signal acquisition, *linear demodulation*[1, 2, 14], and *arctangent demodulation* have been used in many research since they retrieve the body-modulated phase of the radar indicating the chest motion. In fact, in the radar principle, the signal phase can reveal the target displacement in the range of even less than one wavelength; however, it requires to apply a nonlinear function to the signal for the demodulation, which creates strong harmonics if the received signal is contaminated with an interference. More specifically, a practical challenge in phase acquisition of the continuous wave (CW) or frequency-modulated CW (FMCW) radars is the existence of a DC term in the received signal due to multiple reasons such as antenna coupling or RF cross-talk, a stationary object in the desired range, and an intrinsic DC generated by the phase modulation itself[3, 15]. Although all DC components should be eliminated, the DC part of the phase modulation, we call it vital DC, must be in the phase demodulation for a distortionless phase extraction[3]. Otherwise, the vital DC cancellation incurs many harmonics and intermodulations of the breathing and heartbeats in the phase domain[15]. In addition, the phase analysis requires the phase unwrapping, which adds a constraint on how the body moves depending on the sampling frequency[15].

Apart from the signal analysis with implicit ideal assumptions, the radar response, in reality, not only include the target chest motions but also random body activities and the self-movement of radar[4]. For instance, authors in[1, 3] tried to suppress the extra body motions by placing the subject in the middle of two radars or identifying the sudden short-duration movements with the continuous wavelet transform (CWT), respectively. In fact, in[3], the summation of the signals received from two sides of the body effectively cancels the body motions while the respiration and heartbeats remained in the signal. In contrast, in[1], the application of CWT allowed authors to detect interim high-frequency occurring moments corresponding to moderate body motions such as “limb movement" and “crossing the legs". Then, a moving average smooths out the signal in the occurrence of extraneous motions reducing the impact on the detection of vital signs. Furthermore, if the radar platform moves, the authors in[4] proposed a dual-band CW radar such that one band is used to detect the radar motion with respect to a reference reflector.

Essentially, the radar is an integrator, which collects backscattered fields from all reflectors in the environment. For this, the radar observation for a large object, like the human body, is the surface integration of reflected fields on the entire area of the object. Each point on the large target moves with a velocity depending on its relative angles toward the radar. Therefore, even if the mass centre of a large target moves with a constant speed, the radar output will be a signal with many velocity components depending on the relative motions of different points of the target with respect to the radar, the target size, the operating frequency, and a beamwidth of the radar radiation. In fact, the higher the radar resolution is, the lower the integration area is for each *radar cube cell*[16]. Therefore, a radar with high angular and range resolution can select an appropriate part of space in the in 2D (xy) or 3D (xyz) with a reduction in

the distortion due to the smaller integration area. The range resolution depends on the sweeping bandwidth of FMCW chirps, so the higher the range resolution is, the higher RF bandwidth is. Indeed, wideband RF components are expensive, so, there is a tradeoff between the hardware cost and the range resolution. Besides, MIMO radars can obtain a high angular resolution with a few numbers of Tx and Rx antenna elements. In fact, the higher angular resolution is achieved by increasing the effective aperture size of the receiver array, which results in a more compact and cheaper hardware16. So, in this work, we use a MIMO FMCW radar to obtain angular information not only for better signal acquisition but also for detecting a greater number of individuals. In fact, the radar could function as multiple sensors at the same time preserving power, cost, and promoting the safe distancing to COVID-19 patients.

The problem of finding respiration frequency is identical to the classical fundamental frequency estimation where primarily they have been extensively investigated in speech processing17, 18. The problem involves a noisy observation of a signal containing harmonics of a natural process therein the fundamental frequency, magnitude, and the phase of the process are unknown. In fact, depending on the practical considerations, the harmonic mixture is corrupted mainly by an additive Gaussian noise, which in turn a maximum likelihood (ML) estimator17 gives an optimum solution. However, ML requires high computational power and the full knowledge of the noise making it inappropriate to be used in practice. Therefore, there are many traditional sub-optimal harmonic estimators such as linear prediction19, harmonic fitting20, and subspace methods21, 22. Subspace methods use a clever geometrical interpretation of the signal and noise spaces to separate the signal from the noise such as MUltiple SIgnal Classification (MUSIC) analysis12, 23. Furthermore, with the *matched filter* concept, one could find optimum filter coefficients resulting in an output, which is the closest to an ideal noiseless harmonic. In fact, this is implemented by Christensen *et al.*in24, which does not only estimate of the fundamental frequency but also a noiseless waveform. We will apply the high-resolution *optimum filter* when the radar complex signal for each subject is fed into the filter giving the respiration rate and the noiseless waveform. Also, we note that the complex signal detection is more robust than the phase domain analysis since it does not need nonlinear *phase computation*, *phase unwrapping*, and also the *vital DC* cancellation does not create distortions.

For sleep position detection, we collect features from each detected target points as the inputs to support vector machine (SVM) classifier. The detection is novel and does not have any similar prior arts. Knowing the sleep position is much important for patients who could not move from the bed that they usually require to change their sleep position more often as a relief to the bed ulcers. Also, sleep apnea patients need to change their position preceding the obstruction moments. So, the radar advises the patient's supervisor about the sleep position history, and the supervisor helps to change the position of the patient has staid on a position for a long time.

In this work, we use a commercial millimeter-wave FMCW radar by *Texas Instruments*, AWR124325, operating at centre frequency of 79 GHz with 4 GHz sweeping bandwidth. The choice of mm-wave frequency is for high sensitivity in millimeter- scale since the mechanics of the respiration moves the body within a few millimeters15. The radar has 3 transmitters and 4 receivers, but it makes an 8-element

virtual receiver array by the MIMO radar technique. This enables about 14 degrees of angular resolution, which is enough to distinguish two *the same* subjects at 3 meters with 70 cm lateral separation. Furthermore, we use a smart garment, *Hexoksin* vest, by *Carre Technologies inc.* as a reference sensor[26]. It can monitor BR, tidal volume (vt), minute ventilation, and hip motion intensity (HMI) among other vital signs. The authors in[27] reported that the device measures BR for different body postures with 98% accuracy in comparison to the standard laboratory measurement tools. In addition to vital signs monitoring, we propose a novel algorithm for the sleep position detection that determines the position for each individual independently.

Methods

Subjects

Our subjects were selected from healthy people without respiration and heartbeat problems. They participated in our experiment bedrooms at Schlegel University of Waterloo Research Institute for Aging (RIA) in 5 rounds of tests. 3 tests were for breath detection and analysis and 2 experiments were for sleep position detection. The total length of data for the breath and sleep position experiments are 180 and 40 minutes, respectively. In this study, our experiments were conducted based on ethics board approval #31235, which is approved by the Clinical Research Ethics Committee on August 27, 2018. All subjects gave informed consent to participate in the tests. All designed methods conform to the relevant guidelines and regulations.

MIMO radar

Our proposed radar processing involves many steps with the major processing blocks sketched in Fig. 1. The MIMO radar is based on a set of orthogonal transmit waveforms[28]. A particular orthogonal transmission scheme is time division multiplexing (TDM), which creates orthogonality in time by sending signals from only one transmitter at a time. Therefore, at the receiver, the transmitted signals from each transmitter can be separated by knowing that the Rx recording in each time interval corresponds to the transmission from a particular Tx antenna. This separation helps to copy the receiver array based on the transmit element locations. For instance, in Fig. 1b, the transmit array has 2 elements and the receiver has 4 elements. So, the measurement in the second transmission has an additional phase shift with respect to the first chirp depending on the distance of the two transmit antennas. If this distance is equal to the width of the receiver array, so the measurement from the second transmission is equivalent to placing virtual Rx elements next to the actual Rx array –the blue array virtually extends the receiver due to the transmission from the second channel. Theoretically, the virtual 8-element receiver array has the angular resolution of about $2/N = 14.23$ degrees, meaning that two statistically the same targets are resolvable at 3 meters only if they are apart at least 70 centimeters. This is also confirmed with the doll experiments in Fig. 2.

Target detection and breath analysis

Every other chirp is transmitted from a Tx antenna, so the extended array is formed by treating the measured samples of the odd chirps as received by the actual receivers, and the sample of even chirps as received by the virtual receivers. So, at each particular sample index, we have 8 samples across all channels –the actual and virtual channels. The received samples within a chirp period, are then stacked vertically, and the samples across multiple chirps, i.e. slow-time samples, are stacked horizontally. This makes a 3D array called radar cube as shown in Fig. 1b. An FFT is applied to the chirp samples, the vertical direction of the radar cube, to get the signal content in frequency across all virtual channels, which is representing the reflections from different ranges called *range profiles*. The angle of arrival is obtained by exploiting a high-resolution, minimum variance distortion-less response (MVDR) Capon filter on each range bin29. Also, the stationary clutters on each range are removed since the interest is in finding the moving targets.

Then, the constant false alarm rate (CFAR) processor yields a cluster of points corresponding to the moving areas of the targets (see Supplementary Section 2 and Fig. 1a). Also, after clustering, the centre point of each cluster is taken to recover the slow-time respiration signal.

After CFAR, clustering should be able to assign a group of points to one subject. So, the clustering process must determine the number of targets automatically, the mass centre of each target, and it should be computationally efficient. Among many clustering algorithms, we found *mean shift* is fitted to our application with reasonable computation burden. Mean shift requires to know the typical minimum distance of targets, which we set it to 50 cm.

After clustering and finding the centre mass of each target cluster, the waveform of the target extracts from the target range and angle. In fact, the radar cube in Fig. 1b contains the breathing signal of the targets not only at different ranges but also on different azimuths. To extract each target signal individually, the following *angular matched filter* is applied:

$$\mathbf{s}_{ij}(t_s) = w(\tilde{\theta}_j)^H \tilde{\mathbf{x}}(f_{b_i}, t_s) \quad (1)$$

where $\mathbf{s}_{ij}(t_s)$ is the radar response in slow time at the i'th range bin and $\tilde{\theta}_j$ angle. Also, $w(\tilde{\theta}_j)$ is the steering vector for the representative point of the target cluster, and $\tilde{\mathbf{x}}$ is the received vector across all virtual channels after range FFT (see Supplementary Section 1). In fact, $\tilde{\theta}_j$ is angle of the cluster centroid, and $w(\tilde{\theta}_j)$ is formed based on the location of MIMO virtual array. For a linear uniform array with inter-element spacing of d, that is:

$$w(\tilde{\theta}_j) = \left[1 \ \exp\left(j\frac{2\pi}{\lambda} d\sin(\theta_j)\right) \cdots \ \exp\left(j\frac{2\pi}{\lambda}(N-1)d\sin(\theta_j)\right)\right]^T \quad (2)$$

For our radar, the number of virtual channels is $N = 8$, and $d = \lambda/2$. The range of centroids are used to extract the *complex* breathing waveform as an input to the optimum harmonic estimator filter (see Supplementary Section 3).

CFAR and clustering, signal extraction, and other processing parts are frame-based tasks, which are only applied to one frame of data. However, we need to track targets from one frame to another. Therefore, in a new frame, the detected target clusters should be associated to one of the previously found targets if there is no target added or disappeared. This process is called *association*, which has to map new targets in the current frame to the previous frame. Here, we have the following policies for the association:

1. All the current targets should be assigned to the previous targets unless there are more targets than before.
2. If the number of targets in the current frame is greater than before, it assigns the closest targets to the previous ones and add the rest as the new targets.
3. If the number of targets in the current frame is less than before, it assigns the current targets to the previous and freezes the resources in the optimum filters of the disappeared targets for breath analysis.
4. If a target disappears, it holds its optimum filter resources for 2 frames.

After association, the waveform of each target is derived by range and angle filtering. Then, for each target an optimum filter will be dedicated for breath analysis. After target waveform recovery, the optimum filter takes 24 seconds (P) of signal and estimates the respiration rate by sliding the window every 1 second (for definition of the other parameters in optimum filter see Supplementary Section 3). For each detected target, on optimum filter is created.

Sleep position detection

Association and CFAR together provide a collection of points for each target over time. There are features in the points that they have are different if the target sleeps on the back or on the sides. We define features from CFAR points of each subject rather than the radar cube maps, such as range-angle map, to classify each target independently. Our feature selection depends on the target point distributions in space. However, we have observed that Capon CFAR output points are very close in both sleep positions. Unlike slightly different xy point distributions for the two sleep positions, the spatial gradient of the Capon maps is completely different since intuitively the motions around the shoulders drops quicker than around the chest. So, we take a Capon map and apply derivative in both x and y directions laying out two new maps for the x and y derivatives. These derivatives have the following relationship to the range and the angle:

$$dx = \sin(\theta)\, dr + r\cos(\theta)\, d\theta$$

$$dy = \cos(\theta)\, dr - r\sin(\theta)\, d\theta \qquad (3)$$

CFAR points of each target and the corresponding derivatives and the power are features for the target (see Fig. 1b). So, we have *space-time-frequency* features making a 5 dimensional space of {x, y, dx, dy, power}. The feature space suggests that in 5-dimensional space, there is a nonlinear decision boundary for classifying the sleep positions. The data is split into training and test sets with 20% for test set. We used a grid search for hyperparameter optimization of SVM using 5-fold cross validation with the following search space for each parameter.

Results

Dolls

We used two designed dolls to create signal modulation similar to the chest motions of a real human. They are designed in our team with custom motors inside a doll to control moving frequency. They are placed at about 3 meters on two chairs vibrating at two arbitrary frequencies corresponding to 15 and 18 bpm for the target 1 and 2, respectively. In three steps, we made them closer at the same distance to examine the radar capability to distinguish the targets. From test numbers 1 to 3, their distance is reduced laterally. For all tests except test 3, the correct detection of the breathing rate is 100%.

Fig. 2 shows the actual doll placements, the capon maps, and the points cloud derived from CFAR. Although the targets in test 2 are 70 cm apart, they can be distinguished both visually and with CFAR. In fact, theoretically, the minimum distance of two targets at 3 meters should be 70 cm for our radar with an 8-element receiver array, which is confirmed by the test 2 CFAR in Fig. 2h. In contrast, dolls in test 3 are spotted as a single wide point in the Capon map; consequently, CFAR also fails to detect two separate point clouds. This failure is due to the low resolution of the radar in angle, as we mentioned before. Besides, the actual distance of each doll is annotated in Fig. 2. In test 2, two dolls are exactly on the same range. However, their angular separation gives extra freedom to detect their signal independently, as shown in Fig. 2j and Fig. 2k.

Human Subjects

We did experiments in a bedroom with two beds, as shown in Fig. 4a. The subjects were allowed to have a slight motion during sleeping like “sliding the blanket" or “moving hands and legs", but their faces were up toward the radar. The radar and system parameters are listed in the table in Fig. 1a. We will show how the vital signs and sleep positions are obtained in the two experiments. We examined subjects for different sleep positions.

Sleep position detection

In this study, we determine either the patient is sleeping on either right/left sides or on the back facing the radar. The data for training SVM machine learning classifier is collected from two experiments. In each

experiment, two subjects were sleeping on their sides or on backs. Each round was around 20 minutes. For each sleep position, the data length is 40 minutes per target. So, almost the sample size for back and side sleeping are the same.

As mentioned before, the derivative of the Capon map for each target is used as two features (dX and dY). A sample of these maps are shown in Fig. 3b, 3d. They indicate that dX and dY maps are different when a patient is sleeping on the back or on the left side. So potentially, the classifier hardly can determine the two classes. These features are recorded for each target at the vital signs frame rate. Therefore, every frame we have two targets and two samples for the training SVM. For a comparison, the five features are plotted versus each other after standardization process in Fig. 3a using the following relationship:

$$x_{standard} = \frac{x - \bar{x}}{\sigma_x} \qquad (4)$$

where $x_{standard}$ is the standard feature of input x with mean and standard deviation of $\bar{x}$ and σ_x, respectively. In this figure, only 6 views of the feature space are plotted while totally there are $\binom{5}{2}$ = 10 views. By the grid search, the best estimator is found with the parameters listed in Fig. 3c, and the confusion matrix shows at least 83% correct detection of the side or front sleeping (see Fig. 3e).

We conducted three rounds of experiments for two subjects, so, we have 6 subjects in total, who were breathing normally. During these experiments breathing and its waveform were estimated. In each round, two subjects were sleeping for about 20 minutes, and they were sleeping on their back. Fig. 4b shows the output map of CFAR in which the two targets are spotted with point clouds. Although the targets were almost on the same range to the radar, the use of MIMO radar distinguishes them in the angle. Specifically, the left and right subjects are in 1.81 and 1.76 meters to the radar, respectively. In Fig. 4a, the lateral separation of targets was 1 meter, which is enough for the radar angular resolution to resolve the two subjects at this range. At the beginning and at the end of the recording, when the subjects lay down on the bed and when they woke up, their motions are quite high such that the radar signal is highly distorted, and it is not reliable for breathing monitoring as illustrated in Fig. 4c and Fig. 4e. In contrast, in the middle of the test interval, they fell deeper into asleep, and the radar can detect their breathing, as shown in the two figures. The comparison with the reference sensor and the radar shows that the right subject had extra motions at around 130, 177, and 1079 seconds, and this happens for the left subject at around 84, 264, and 936 seconds, which are encircled in Fig. 4c and Fig. 4e.

Using *optimum filter* does not only enhance and separate periodic signals, but it provides an estimate of the signal waveform as well. As illustrated in Fig. 4d and Fig. 4f, the radar signal contains many harmonics due to reasons as we discussed before. However, the filter output is a noiseless waveform corresponding to a single frequency signal with the frequency of breathing rate, which is labeled in the figures with *reconstructed signal*. The magnitude of signals is related to the thorax displacement in a respiration cycle, which represents the lung volume change.

To show the breathing detector for another sleep position, Fig. 5 demonstrates a measurement result in the same room shown in Fig. 4a where a patient slept on her side for about 20 minutes. Although the patient was aware that she should not move during recording, she was told to feel free if she wants to quickly move. Body motions creates frequency components interfering with BR frequencies. As a result, the radar BR estimator in the moments subject moves should be discarded, and they are marked in Fig. 5a with circles. Also, a sample of the side sleeping breathing waveforms is shown in 5b similar to what is shown in Fig. 4d, 4f.

The system performance is evaluated based on two metrics: average error rate and root mean square error (RMSE). The former represents the error when the BR estimated by the radar is not closer than 3 bpm to the true value, and the later gives the error standard deviation in bpm. The average of the metrics for all experiments are illustrated in Fig. 5c. In all analysis, the moments with body motions are eliminated. The BR correct detection rate for left and right subjects sleeping on back are 99% and 94%, respectively. Also, the side sleeping has even lower error rate than the back sleeping for the right target, and the detection rate is 99% in this case. Overall, our system shows 97% accuracy in respiration rate analysis. In addition, RMSE values imply that the radar detection has maximum 1.7 bpm deviation over a long period.

Discussion

We proposed and developed a system for bedbound patients to monitor breath and their sleep positions. The novel algorithm detects closely spaced sleeping subjects with a single radar and analyzes them individually. This advantage is due to using an array at the receiver whereas we achieve a higher number of target detection by virtually extending the number of receiver elements with using MIMO radar. Therefore, instead of using multiple sensors per patient, which are having a single functionality of either monitoring breathing or sleep position, we employed a single radar to carry out those measurements. Replacing all the conventional sensors with only one sensor reduces the cost, power while maintaining reliable accuracy. The proposed system has two monitoring tasks: breathing and sleep position. For breathing, a spectral estimator was designed with 1 bpm resolution and the update rate of 1 second to estimate the breathing rate and its noiseless waveform. For sleep position detection, an SVM machine learning classifier with appropriate set of features proposed to determine the side or back sleeping for each patient independently. The system was also tested by two designed dolls to show how targets can be close in angle and the ability of the harmonic estimator to extract independent breath-like signals from the two dolls. They were as close as 70 cm and about 3 meters to the radar. The radar was 100% successful to detect the vibration frequency of the dolls. Moreover, the bedroom experiments validated the system performance in a practical setting. The sleep position detector was successful more than 83%. Also, the breathing rate accuracy tested for two different sleep positions. For the back sleeping, the breathing rate was at least 94% of time closer than 1 bpm to the reference sensor. This was 99% for side sleeping. In addition, considering all measurements, the maximum RMSE of breathing rate was 1.7 bpm. The Discussion should be succinct and must not contain subheadings.

Declarations

Acknowledgements

This work was supported by the Natural Science and Engineering Council (NSERC) of Canada, the Ontario Centers of Excellence (OCE), and the Schlegel Research Institute for Aging (RIA). The authors would like to thank Ms. Clara Magnier, Mr. Tom Paraschuk, and Ms. Mariam Laghi Mrabat for voluntarily helping for the data collection and measurement campaigns.

Author contributions statement

Conception, data analysis and representation, and manuscript writing: M. A. Design of the work, data collection and conducting experiments, and manuscript review and editing: G. S. Manuscript review and editing: S. S. N.

Competing interests

The authors declare no competing interests.

Additional information

Supplementary materials are available on the *scientific reports website*.

Correspondence and request of materials should be addressed to M. Alizadeh.

References

1. Mercuri, *et al.* Vital-sign monitoring and spatial tracking of multiple people using a contactless radar-based sensor. *Nat. Electron.* **2**, 252–262, DOI: 10.1038/s41928-019-0258-6. Number: 6 Publisher: Nature Publishing Group.
2. Droitcour, D. *Non-Contact Measurement of Heart and Respiration Rates with a Single-Chip Microwave Doppler Radar* (2006).
3. Li, & Lin, J. Random body movement cancellation in doppler radar vital sign detection. *IEEE Transactions on Microw. Theory Tech.* **56**, 3143–3152, DOI: 10.1109/TMTT.2008.2007139 (2008).
4. Zhu, , Wang, K. & Wu, K. A fundamental-and-harmonic dual-frequency doppler radar system for vital signs detection enabling radar movement self-cancellation. *IEEE Transactions on Microw. Theory Tech.* 1–13, DOI: 10.1109/TMTT.2018. 2869591 (2018).
5. Nahar, *et al.* An electromagnetic model of human vital signs detection and its experimental validation. *IEEE J. on Emerg. Sel. Top. Circuits Syst.* **8**, 338–349, DOI: 10.1109/JETCAS.2018.2811339 (2018).
6. Li, , Xiao, Y. & Lin, J. Experiment and spectral analysis of a low-power kaka-band heartbeat detector measuring from four sides of a human body. *IEEE Transactions on Microw. Theory Tech.* **54**, 4464–

4471 (2006).

7. Gabriel, , Gabriel, S. & Corthout, E. The dielectric properties of biological tissues: I. literature survey. *Phys. Medicine Biol.* **41**, 2231–2249, DOI: 10.1088/0031-9155/41/11/001.
8. Gabriel, , Lau, R. W. & Gabriel, C. The dielectric properties of biological tissues: II. measurements in the frequency range 10 hz to 20 GHz. *Phys. Medicine Biol.* **41**, 2251–2269, DOI: 10.1088/0031-9155/41/11/002.
9. Gabriel, , Lau, R. W. & Gabriel, C. The dielectric properties of biological tissues: III. parametric models for the dielectric spectrum of tissues. *Phys. Medicine Biol.* **41**, 2271–2293, DOI: 10.1088/0031-9155/41/11/003.
10. Lee, , Kim, B.-H., Park, J.-K. & Yook, J.-G. A novel vital-sign sensing algorithm for multiple subjects based on 24-GHz FMCW doppler radar. *Remote. Sens.* **11**, 1237, DOI: 10.3390/rs11101237.
11. Shyu, , Chiu, L., Lee, P., Tung, T. & Yang, S. Detection of breathing and heart rates in uwb radar sensor data using fvpief-based two-layer eemd. *IEEE Sensors J.* **19**, 774–784, DOI: 10.1109/JSEN.2018.2878607 (2019).
12. Kim, & Lee, K. Low-complexity joint extrapolation-music-based 2-d parameter estimator for vital fmcw radar. *IEEE Sensors J.* **19**, 2205–2216, DOI: 10.1109/JSEN.2018.2877043 (2019).
13. Wang, *et al.* Noncontact heart rate measurement based on an improved convolutional sparse coding method using ir-uwb radar. *IEEE Access* **7**, 158492–158502 (2019).
14. Park, , Boric-Lubecke, O. & Lubecke, V. M. Arctangent demodulation with DC offset compensation in quadrature doppler radar receiver systems. *IEEE Transactions on Microw. Theory Tech.* **55**, 1073–1079, DOI: 10.1109/TMTT.2007.895653.
15. Alizadeh, , Shaker, G., Almeidaand P. P. Morita, J. C. M. D. & Safavi-Naeini, S. Remote monitoring of human vital signs using mm-wave fmcw radar. *IEEE Access* **7**, 54958–54968 (2019).
16. Alizadeh, , Abedi, H. & Shaker, G. Low-cost low-power in-vehicle occupant detection with mm-wave FMCW radar. In *2019 IEEE SENSORS*, 1–4, DOI: 10.1109/SENSORS43011.2019.8956880. ISSN: 1930-0395.
17. Christensen, & Jakobsson, A. *Multi-Pitch Estimation* (Morgan and Claypool Publishers).
18. Noll, M. Cepstrum pitch determination. *The J. Acoust. Soc. Am.* **41**, 293–309, DOI: 10.1121/1.1910339.
19. Chan, W. & So, H. C. Accurate frequency estimation for real harmonic sinusoids. *IEEE Signal Process. Lett.* **11**, 609–612, DOI: 10.1109/LSP.2004.830115.
20. Li, , Stoica, P. & Li, J. Computationally efficient parameter estimation for harmonic sinusoidal signals. *Signal Process.* **80**, 1937–1944, DOI: 10.1016/S0165-1684(00)00103-1.
21. Christensen, M. G., Jakobsson, A. & Jensen, S. H. Fundamental Frequency Estimation using the Shift-Invariance Property. In *2007 Conference Record of the Forty-First Asilomar Conference on Signals, Systems and Computers*, 631–635, DOI:1109/ACSSC.2007.4487290 (2007).

22. Christensen, G., Jakobsson, A. & Jensen, S. H. Joint high-resolution fundamental frequency and order estimation. *IEEE Transactions on Audio, Speech, Lang. Process.* **15**, 1635–1644, DOI: 10.1109/TASL.2007.899267. Conference Name: IEEE Transactions on Audio, Speech, and Language Processing.
23. Christensen, G. & Jakobsson, A. Optimal filter designs for separating and enhancing periodic signals. *IEEE Transactions on Signal Process.* **58**, 5969–5983, DOI: 10.1109/TSP.2010.2070497.
24. Li, & Lin, J. Optimal carrier frequency of non-contact vital sign detectors. In *2007 IEEE Radio and Wireless Symposium*, 281–284, DOI: 10.1109/RWS.2007.351823. ISSN: 2164-2974.
25. AWR1243boost AWR1243 76-GHz to 81-GHz high-performance automotive MMIC evaluation module | com.
26. inc (Hexoskin), T. Hexoskin Smart Shirts - Cardiac, Respiratory, Sleep & Activity Metrics.
27. Villar, , Beltrame, T. & Hughson, R. L. Validation of the Hexoskin wearable vest during lying, sitting, standing, and walking activities. *Appl. Physiol. Nutr. Metab. Appliquee, Nutr. Et Metab.* **40**, 1019–1024, DOI: 10.1139/apnm-2015-0140 (2015).
28. Hassanien, & Vorobyov, S. A. Phased-MIMO radar: A tradeoff between phased-array and MIMO radars. *IEEE Transactions on Signal Process.* **58**, 3137–3151, DOI: 10.1109/TSP.2010.2043976.
29. Capon, High-resolution frequency-wavenumber spectrum analysis. *Proc. IEEE* **57**, 1408–1418, DOI: 10.1109/PROC. 1969.7278.

Figures

Parameters	Radar Configuration Parameters				Range CFAR			Azimuth CFAR			Optimum Filter			
	K	B_{eff}	T_c	T_f	P_{fa}	N_g	N_t	P_{fa}	N_g	N_t	P	Q	L	Δf
Values	98 MHz/μs	1.782GHz	580 μs	40ms	0.3	4	22	0.4	4	40	24	8	1	1 bpm

(a) Radar system parameters

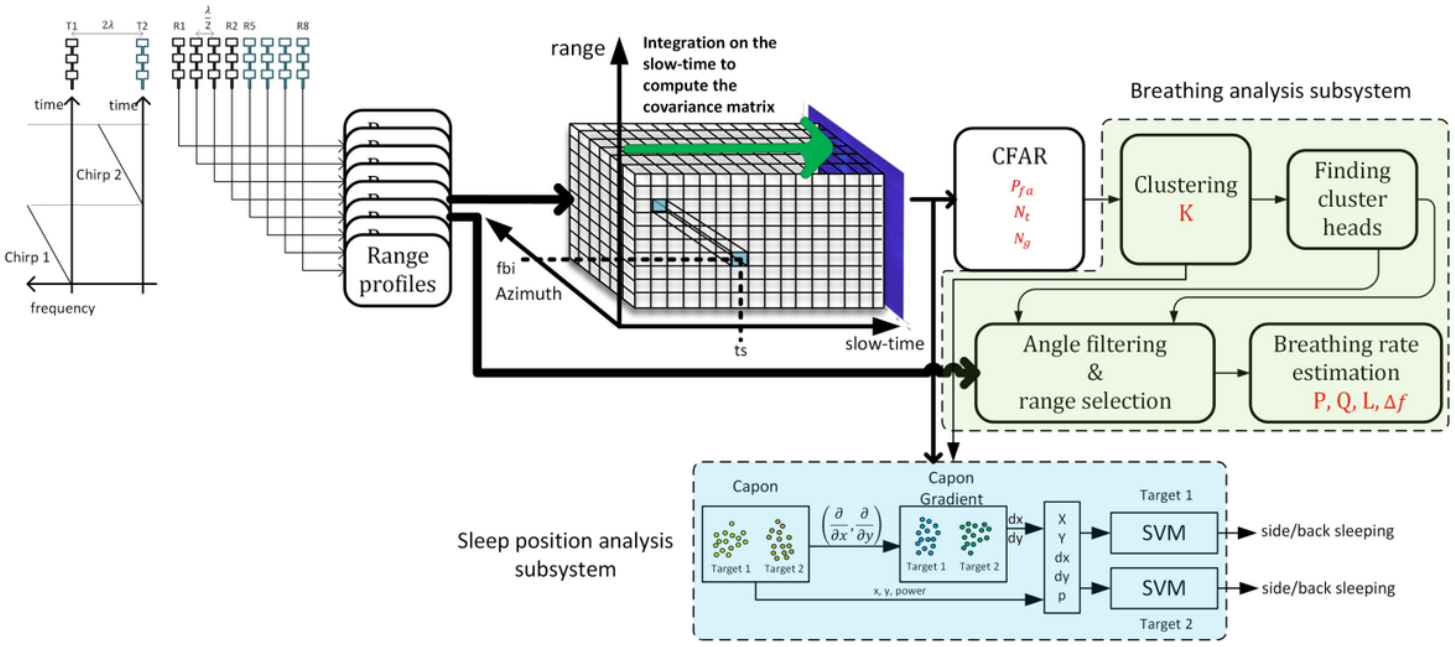

(b) Signal processing flow and the parameters

Figure 1

System architecture: (a) system parameters, (b) signal processing chain

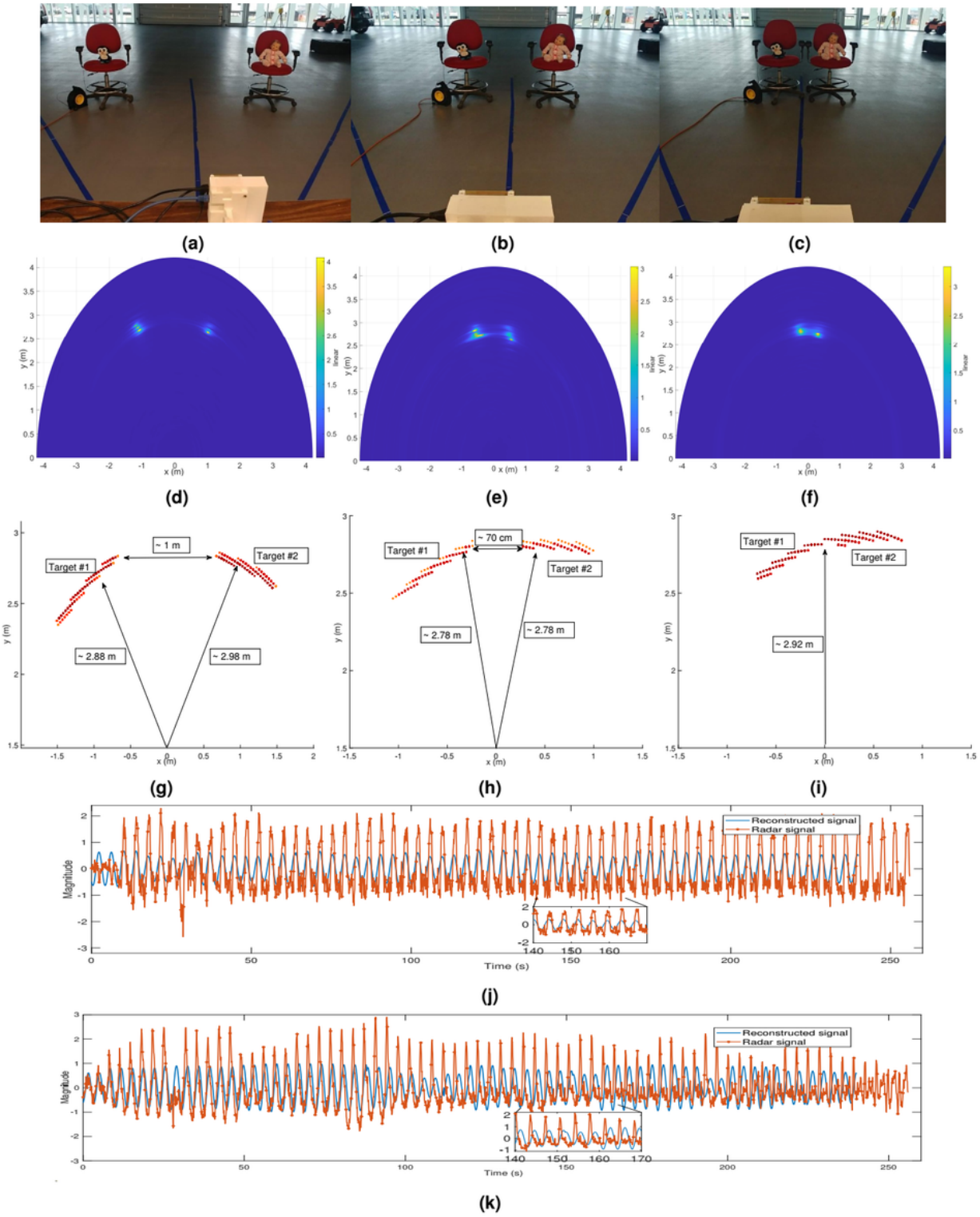

Figure 2

Doll tests with numbers 1,2,3 from left to right: a-c) 3 settings for doll positions with different angular separations, d-i) Capon range-azimuth maps and their CFAR point clouds, j-k) sample breathing waveforms for the left and right dolls in test 2. For the test 1,2, and 3, the side-by-side distances are 1 meter, 70 centimeters, and less than 70 centimeters, respectively.

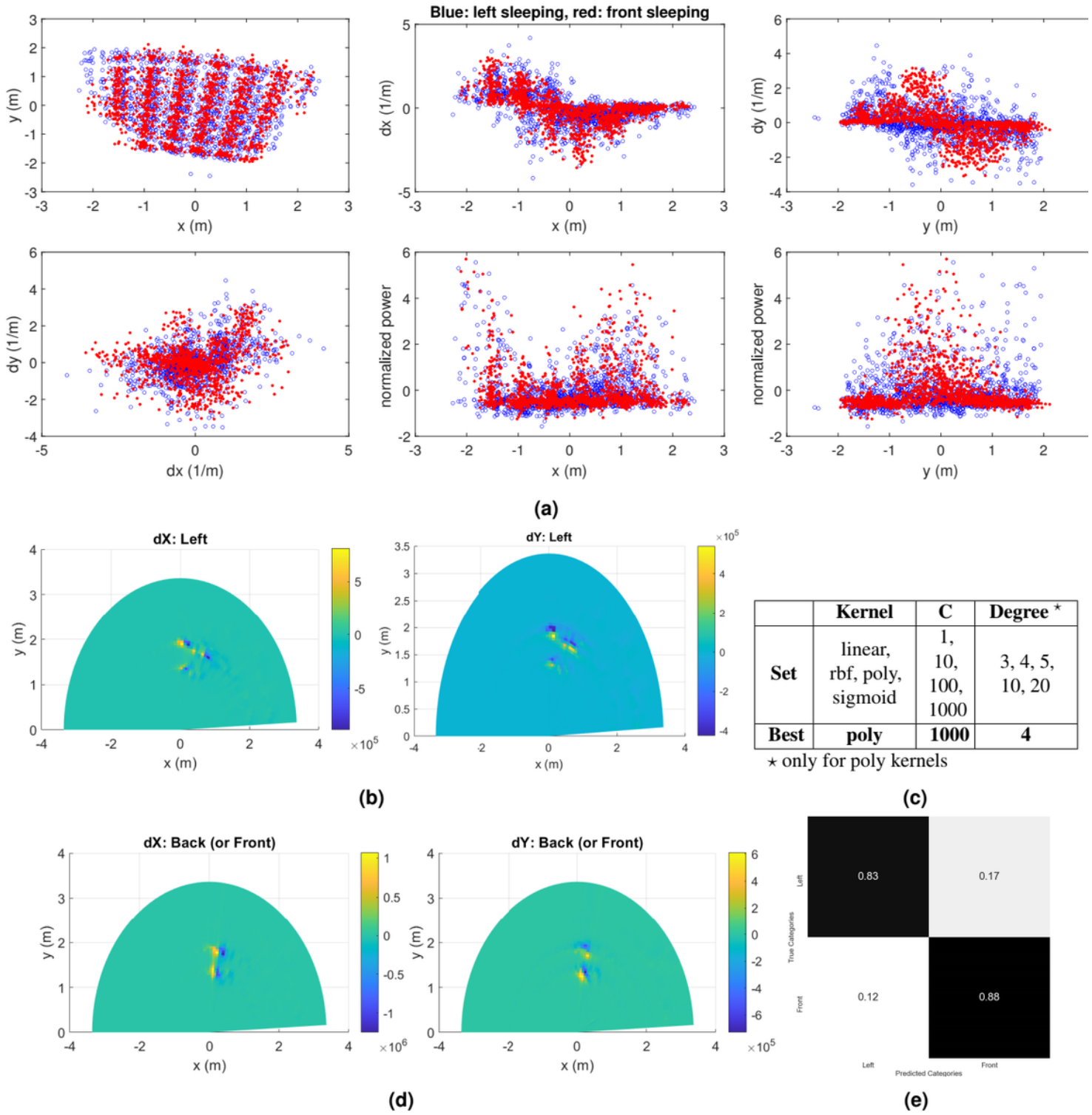

	Kernel	C	Degree ⋆
Set	linear, rbf, poly, sigmoid	1, 10, 100, 1000	3, 4, 5, 10, 20
Best	**poly**	**1000**	**4**

⋆ only for poly kernels

(c)

Figure 3

Sleep position classification: (a) point clouds of the feature space, (b,d) Capon gradient sample maps, (c) hyperparameter tuning, (e) confusion matrix of the best SVM classifier.

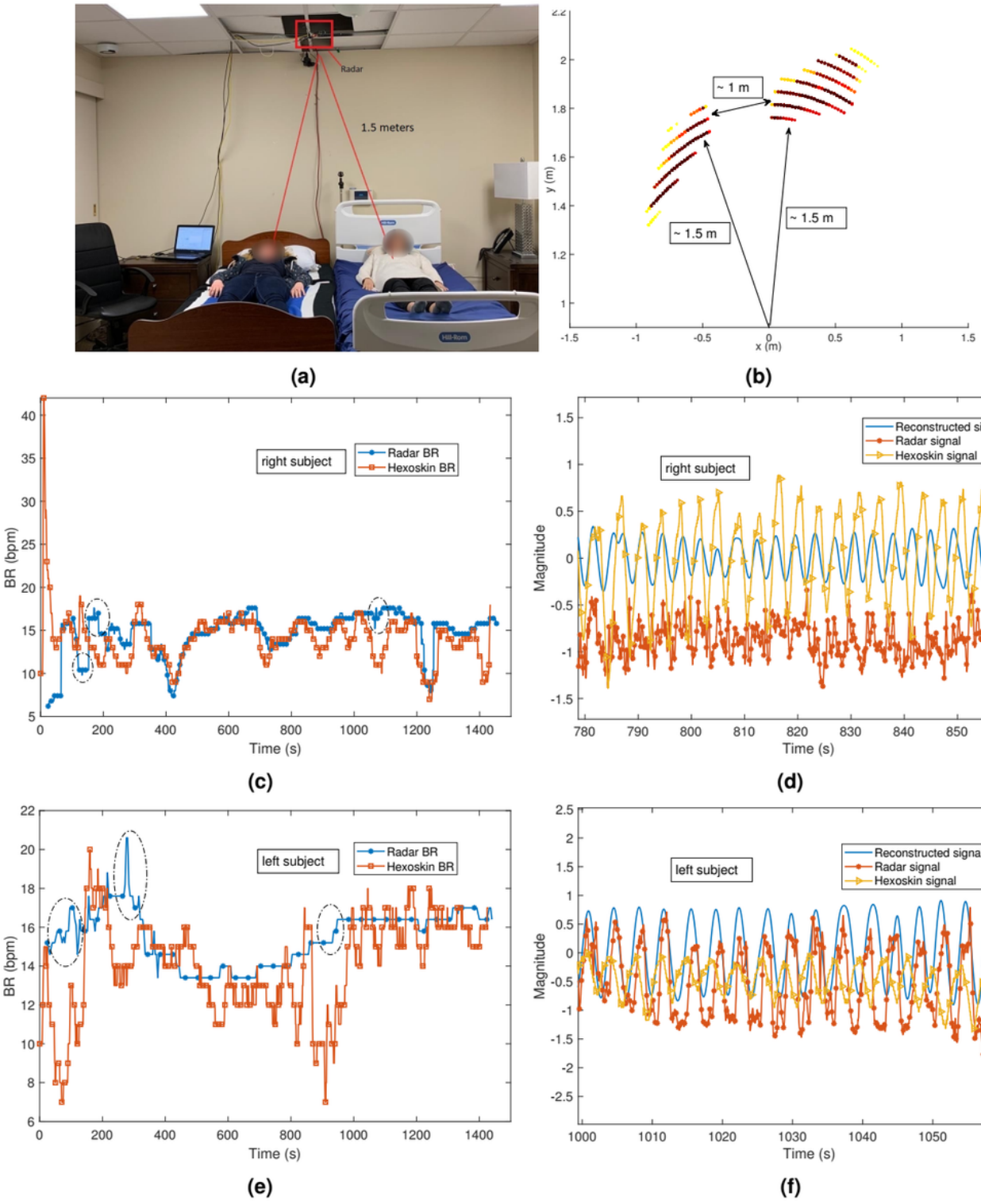

Figure 4

Human subject study results: (a) bedroom, (b) CFAR points, (c, e) breathing rate time traces and Hexoskin, (d, f) breathing waveforms for the radar, optimum filter output, and the Hexoskin.

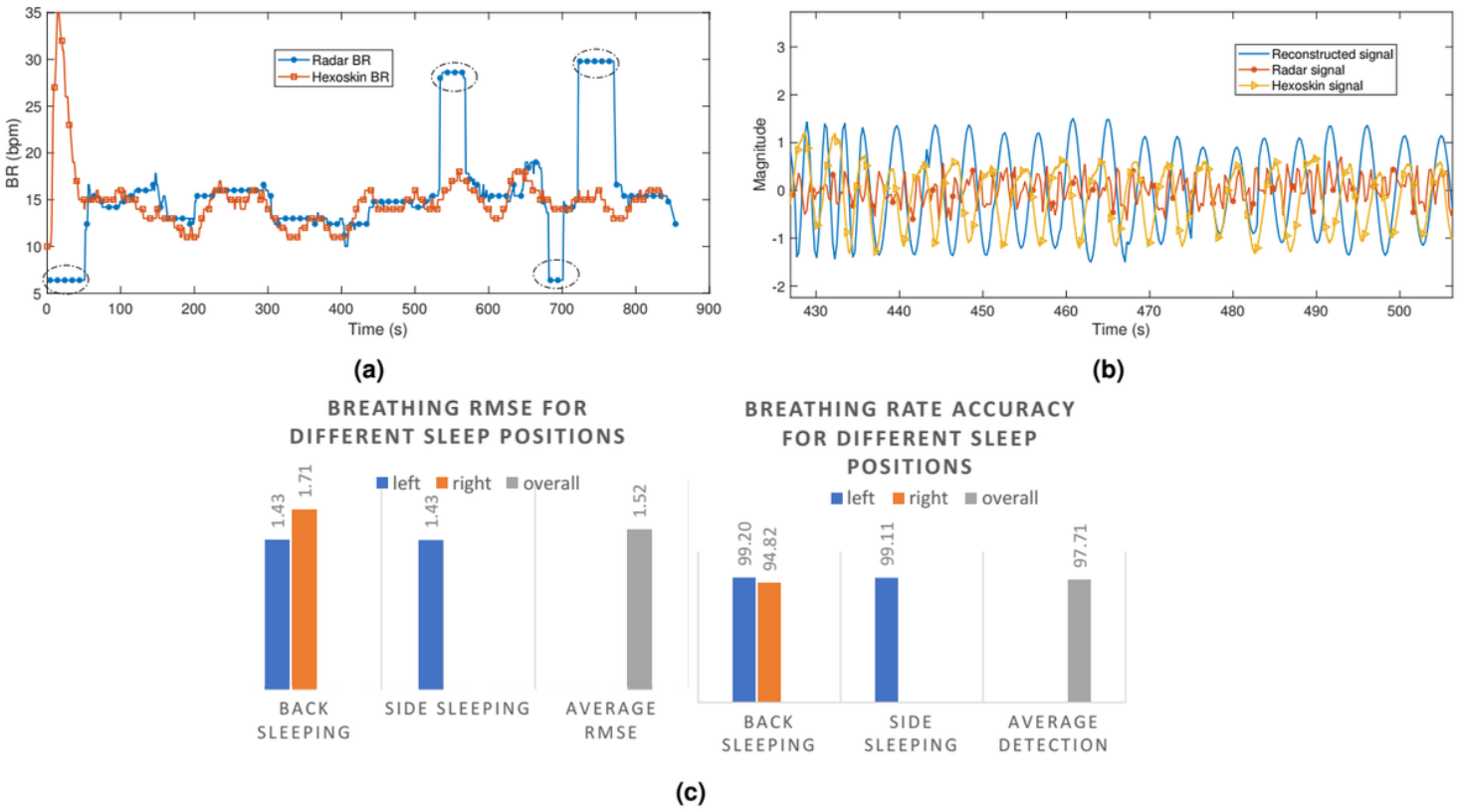

Figure 5

Breathing rate results for sleeping on the left side: (a) breathing rate time traces for the radar and the reference sensor, (b) breathing waveforms for the radar, optimum filter output, and the Hexoskin, (c) breath rate detection performance for different sleep positions.

Supplementary Files

This is a list of supplementary files associated with this preprint. Click to download.

- mainsupp1.pdf
- sample2.mp4